# Dielectric based resonant guided wave networks

**Eyal Feigenbaum[1,*] and Harry A. Atwater[1]**

[1]*Thomas J. Watson Laboratory of Applied Physics, California Institute of Technology, Pasadena, California 91125, USA*

[*]*eyalf@caltech.edu*

**Abstract:** Resonant guided wave networks (RGWNs) are demonstrated to operate based on dielectric waveguides, broadening the scope of this optical design approach beyond plasmonics. The intersection of two dielectric waveguides that is modified by a tuned scattering particle is shown to function as an equal power splitting element, a key enabler of resonant guided wave networks. We describe structures composed of two types of waveguides, Si slabs and SOI ribs, at the telecom frequencies using both, Au and etch, based scatterers.



**OCIS codes:** (160.4670) Optical materials; (160.3918) Metamaterials.

## References and links

1. E. Yablonovitch, "Photonic crystals: semiconductors of light," Sci. Am. **285**(6), 46–55 (2001).
2. J. D. Joannopoulos, S. G. Johnson, J. N. Winn, and R. D. Meade, *Photonic Crystals: Molding the Flow of Light*, 2nd ed. (Princeton, 2008).
3. V. M. Shalaev, "Optical negative-index metamaterials," Nat. Photonics **1**(1), 41–48 (2007).
4. J. B. Pendry, D. Schurig, and D. R. Smith, "Controlling electromagnetic fields," Science **312**(5781), 1780–1782 (2006).
5. E. Feigenbaum and H. A. Atwater, "Resonant guided wave networks," Phys. Rev. Lett. **104**(14), 147402 (2010).
6. E. Feigenbaum, S. P. Burgos, and H. A. Atwater, "Programming of inhomogeneous resonant guided wave networks," Opt. Express **18**(25), 25584–25595 (2010).
7. W. L. Barnes, A. Dereux, and T. W. Ebbesen, "Surface plasmon subwavelength optics," Nature **424**(6950), 824–830 (2003).
8. E. Feigenbaum and M. Orenstein, "Modeling of Complementary (Void) Plasmon Waveguiding," J. Lightwave Technol. **25**(9), 2547–2562 (2007).
9. E. Feigenbaum and M. Orenstein, "Perfect 4-way splitting in nano plasmonic X-junctions," Opt. Express **15**(26), 17948–17953 (2007).
10. H. A. Atwater and A. Polman, "Plasmonics for improved photovoltaic devices," Nat. Mater. **9**(3), 205–213 (2010).
11. Transmission to TE1 is calculated using point monitor at the center of the waveguide for the Ez component (where TE2 amplitude is zero). The total transmission is calculated using a line monitor across the waveguide and integrating over the power normal to it.
12. E. D. Palik, *Handbook of Optical Constants of Solids*, 2nd ed. (Academic, 1998).

## 1. Introduction

Recently, a new class of optical artificial materials [1–4], known as resonant guided wave networks (RGWNs), was reported [5]. In resonant guided wave networks, localized waves resonate in closed paths throughout a network of isolated waveguides connected by wave splitting elements. The resulting network resonances give rise to wave dispersion that is sensitive to the network layout. As a design paradigm, resonant guided wave networks are based on the underlying physics of waveguides and waveguide junctions, and to date resonators, band-gap materials [5] and devices with programmable optical transmission properties have been demonstrated [6]. Resonant guided wave networks can be viewed essentially as a method for discrete transformation optics [4], since the matrix linking RGWN inputs and outputs has a compact mathematical representation [6], which enables the mapping of desired optical transformations to a network layout.

A resonant guided wave network is comprised of power splitting elements connected by isolated waveguides, as illustrated in Fig. 1(a). The function of each splitting element is to

#163588 - $15.00 USD Received 23 Feb 2012; revised 26 Mar 2012; accepted 26 Mar 2012; published 24 Apr 2012

distribute the wave entering any of its terminals between all of its terminals, with a prescribed transmission phase and amplitude (see Fig. 1(b)). Waves then propagate in isolated waveguides between splitting elements, where waves localized in different input waveguides are coupled. By controlling the properties of each splitting element and every waveguide, the network intereference and resonances can be determined and thus also the optical function of the network. This allows for a compact design of complex interferometric devices, such as color routers [6] or possibly of mode converters.

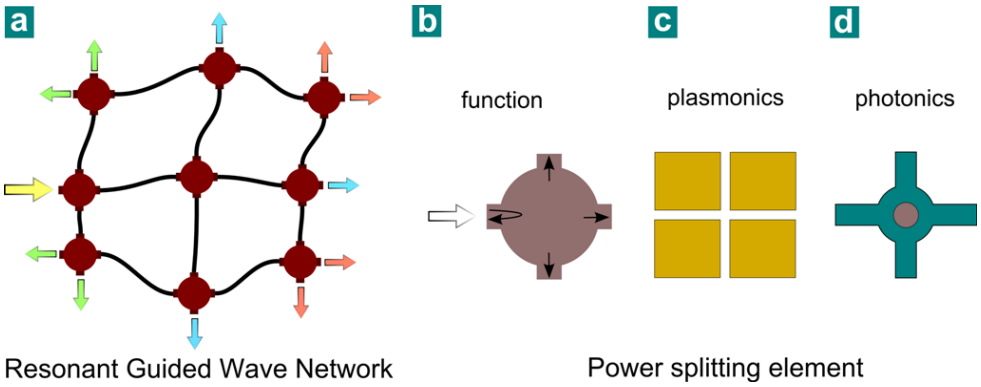


Fig. 1. Illustration of resonant guided wave networks (RGWNs): a) RGWN composed of nine power splitting elements which functions as a color router; b) power splitting of an incoming wave between the four terminals; c) implementation of the power splitting element for the plasmonic mode in two intersecting MIM waveguides; d) a possible implementation for photonic modes based on modifying the intersection with a scattering particle.

A key enabling component of a resonant guided wave network is the power splitting element. This element operates counter intuitively to the intersection of two conventional photonic waveguides, for which the majority of the power ordinarily couples into the forward terminal. It was found that at the intersection of two metal-insulator-metal (MIM) waveguides [7,8], (see Fig. 1(c)) with subwavelength inter-metal gap spacing, the power splits equally between the outputs. This distinctive behavior stems from the slow wave nature of the plasmonic mode propagating in metal-insulator-metal waveguides, which has a mode profile comprised of many higher wave vector components [9].

Since plasmonic structures inherently support design of power splitting elements, it is straightforward to show that a network of intersecting metal-insulator-metal waveguides can give rise to a resonant guided wave network. An idealized two-dimensional (2D) plasmonic network of air grooves in a Au matrix was demonstrated with full wave electromagnetic simulations [5]. While a plasmonic resonant guided wave network has a simple topology and operates over a broad range of frequencies, it suffers from significant attenuation due to material loss and from lesser compatibility with dielectric-based integrated photonic technologies.

We report here designs for resonant guided wave networks that do not rely on plasmonic structures but rather on standard dielectric waveguides. Such dielectric resonant guided wave networks could mitigate the inherent losses of plasmonic structures and enable integration with more commonly used components of photonic circuitry.

## 2. Power splitting at the intersection of two waveguides without scatterers

We start by studying the scattering junction at the intersection of two dimensional slab waveguides. The emphasis here is to achieve equal power splitting at the waveguide intersection, since this presents the main barrier for achieving resonant guided wave networks with dielectric modes. We employ a scattering particle to increase the coupling into the side terminal, which is intuitive from the standpoint of momentum matching, and has also been

#163588 - $15.00 USD Received 23 Feb 2012; revised 26 Mar 2012; accepted 26 Mar 2012; published 24 Apr 2012

suggested for light trapping in thin solar cells [10]. We investigate the scattering elements and the conditions that enable power splitting as a proof of concept and also to obtain a clearer understanding of the underlying physics. We first examine idealized two-dimensional configurations, where the TE and TM mode families are decoupled. Three-dimensional structures, and their associated challenges, will be discussed in section 4.

For simplicity, we will use high contrast slab waveguides, of air-Si at the telecommunication frequencies (1.5μm free space wavelength). We limit the discussion in this work to cases where the slab waveguide thickness supports the propagation of only one mode with higher order modes cut-off, since the use of waveguides that support propagation of more than one mode could lead to mode conversion.

The effective indices of the different modes (i.e., the ratio between their wave momentum and free space momentum) as a function of waveguide width are given in Fig. 2(a). The propagation of the second TE mode (TE2) is enabled for waveguide thicknesses above 230 nm, which sets the upper limit on the slab thickness used here. For waveguide thicknesses of less than 300 nm, only the lowest TM mode (TM1) propagates. Since the two polarizations are decoupled in the 2D configurations, we will examine separately the excitation by the two lowest modes (i.e., TE1 and TM1).

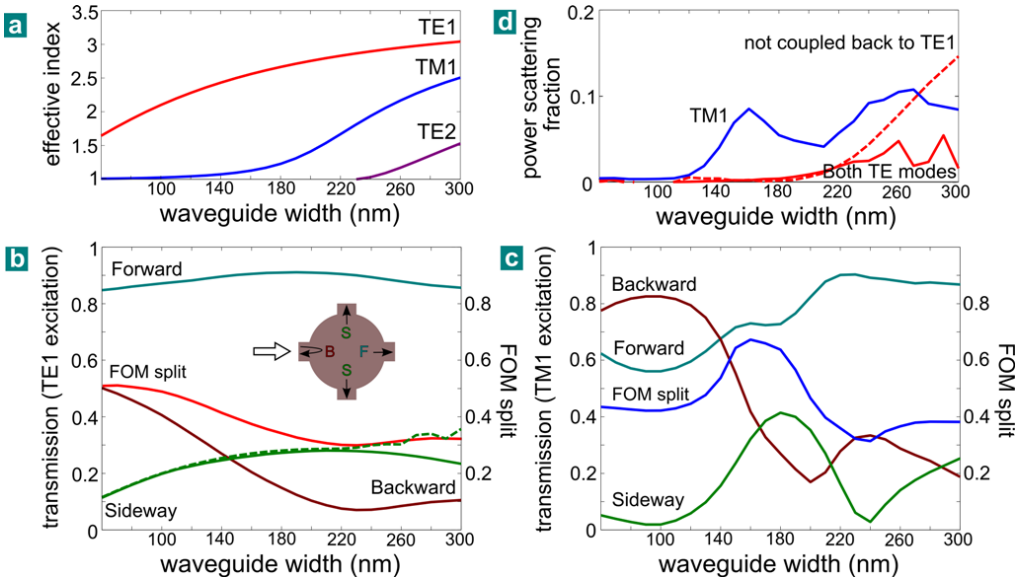


Fig. 2. Power splitting at the intersection of two equal width Si-air slabs without a scattering element at λ = 1.5 μm as a function of their width: a) effective index of the slab modes; field transmission to the different terminals and the FOM for equal power splitting for (b) TE1 and (c) TM1 excitation; d) the fraction of scattered power for TM1 (blue) and TE1 (red) excitation (see Appendix A for more details).

For two normal intersecting slab waveguides without a scattering element at the junction, the side coupling is not high enough to allow for equal optical power splitting. In Fig. 2(b), the field transmission to the different terminals is given as a function of the waveguide width for TE1 excitation at one of the terminals of the waveguides intersection. We examine only cases with equal thickness waveguides to maintain the symmetry required for achieving equal power splitting with excitation from any of the terminals. The solid curves in Fig. 2(b), only show the field transmission to the TE1 mode for the different terminals, whereas the (green) dashed curve indicates the total power side transmission (to all the TE modes) [11]. The two green curves (dashed and solid) differ for slab widths that are larger than 230 nm, resulting in the appearance of the TE2 mode, as could be also correlated with the data in Fig. 2(a). To monitor the transmission to all terminals at once, we examine the figure of merit (FOM) for

#163588 - $15.00 USD Received 23 Feb 2012; revised 26 Mar 2012; accepted 26 Mar 2012; published 24 Apr 2012

power splitting: $FOM_{split} = 1 - \frac{2}{3}\left(\left|T_f - \frac{1}{2}\right| + \left|T_s - \frac{1}{2}\right| + \left|T_b - \frac{1}{2}\right|\right)$, which ranges between 0 and 1, where 1 corresponds to equal power splitting ($T_f$, $T_s$, and $T_b$ are field transmission to the forward, sideways and backwards terminals). Finite difference time domain (FDTD) simulations (numerical calculations done using the commercial code FDTD solutions from Lumerical) demonstrate that even though the TE2 cut-off slab thickness is indeed 230nm, for narrower slabs with thickness values between 190 nm and 230 nm there is still side coupling to the TE2 as leaky modes. This is manifested in the simulations by a local beating pattern between the TE1 and TE2 modes in the vicinity of the intersection (and vanishes ~1-2 wavelengths away from the junction). Additionally, the increase in side power transmission saturates for widths just below 200 nm. These considerations led us to choose the nominal slab width to be approximately 180 nm. Nevertheless, even for these settings the side coupling is substantially lower than that required for power splitting.

In the case of TM1 excitation, we are able to achieve more uniform power splitting for waveguide widths of 180 nm, according to the results in Fig. 2(c). The different behavior observed for TM1 may be due to a difference in the cross-sectional mode profiles of the two mode families, which weight differently the confinement (e.g., the spatial k-components population) between the increase in the waveguide thickness versus the increase in the confinement to the waveguide core with the effective index. Although four-way transmission can be achieved for TM1 mode excitation in the d = 180nm waveguide intersection, it suffers from substantial power scattering as observed from Fig. 2(d). In addition, in three-dimensional resonant guided wave networks, because of coupling of the two polarizations, excitation of the higher index mode is preferable (in this case, the TE1 mode rather than the TM1), since the high index is less likely to couple to the lower effective index modes and therefore to maintain the equal power splitting within the same mode. These characteristics of dielectric waveguide junctions without scatterers are substantially inferior those obtained in plasmonic waveguide junctions (see Fig. A1 in Appendix B). All of these reasons motivate addition of a scattering element at the waveguide junction.

### 3. Two dimensional analysis of dielectric-based resonant guided wave networks

Two types of circular scattering elements were examined: a metallic circle and a dielectric circle with a high refractive index contrast, both encapsulated in a cladding layer (as illustrated in Fig. 1(d)). The role of the scattering element is to increase the coupling to the side and backwards terminals. The cladding layer increases the coupling to the forward terminal and thus allows the use of large scattering elements, with diameters greater than the waveguide width. Our goal here is to find the conditions that allow for equal power splitting. The intersection of the two Si slab waveguides is modified by two types of circular scattering elements, composed of Au and of air, both with a ring-shaped cladding layer of Si.

The addition of a Au scattering element to the intersection of the two 180 nm slab waveguides enables the equal power splitting of an incoming TE1 wave. The side transmission approaches its desired value of 0.5 and $FOM_{split}$ of 1 for a scattering radius of 60 nm, as illustrated in Fig. 3(a). The simulations presented here, and throughout this paper, use experimentally tabulated values of the complex refractive index of the materials [12]. In comparison, the highest value of this $FOM_{split}$ for the particle free junction is 0.5 and 0.67 for TE1 and TM1 excitations, accordingly (see Fig. 2). The Si cladding layer thickness does not seem to substantially affect the result, perhaps since a metal particle with 120 nm diameter leaves enough space for the wave in the 180 nm waveguide to traverse around it. The fraction of scattered power in the wave splitting is relatively small for the assumed scattering dimensions (~3%), as seen in Fig. 3(b). Even though we focus our efforts in this paper on achieving perfectly equal power splitting, this figure demonstrates clearly the broad parameter space that is achievable. This parameter space can be conceptually divided into three regions according to Fig. 3(a) and Fig. 3(b): the upper right corner of these figures where the

#163588 - $15.00 USD Received 23 Feb 2012; revised 26 Mar 2012; accepted 26 Mar 2012; published 24 Apr 2012

scattering is dominant; the lower right corner where the wave continues mostly unaffected by the junction; and the left region of the figures where the junction operates as a power splitter.

It is also interesting to ask whether dielectric-based power splitting elements can achieve broadband operation, as is possible for plasmonic structures [9]. The power splitting bandwidth is calculated as the full-width-half-maximum (FWHM) of the side terminal transmission when the junction is excited with a broadband TE1 pulse, which is illustrated in Fig. A2(a) in Appendix B. For a scattering element radius of 60 nm, the maximal bandwidth is achieved when there is essentially no cladding layer (thickness < 30 nm), and is about 277 THz. This is a substantial bandwidth, yet smaller than the ~400THz bandwidth achieved for plasmonic structures (see Fig. A1(c) in Appendix B). Broadband power splitting is evident from Fig. 3(c) (see also Media 1 to watch the dynamics), as a pulse of only few optical cycles equally splits at the junction of two 180 nm wide Si slab waveguides with a 60 nm radius Au particle.

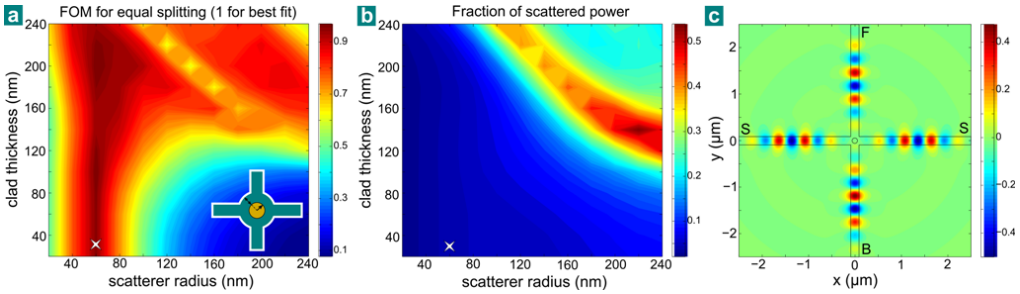


Fig. 3. Power splitting at the intersection of two 180nm wide Si-air slabs modified by a radial Au particle at the junction: (a) FOM of equal splitting and (b) Fraction of scattered power as a function of the Au particle radius and the Si cladding layer thickness. c) snapshot of the E-field out-of-plane component at the incidence of equal power splitting for a pulse excitation with the lowest TE polarization mode from terminal 'B' (Media 1). The intersection of the two 180 nm Si slabs is modified with a 60 nm radius Au particle as indicated by the structure overlay, and also by a white star on the parameter space in figures 'a' and 'b'. $\lambda = 1.5\mu m$.

Another notable property of power splitting elements is the phase difference between the outgoing waves at the different terminals. This phase difference is an important factor for designing the interference in resonant guided wave networks. The desired phase distribution of the power splitting elements in the network depends on the desired optical function. For example, an enhanced resonator quality factor *Q* was obtained in plasmonic resonant guided wave networks with square topology when the side traveling and forward traveling waves were approximately in-phase and are out-of-phase, respectively, (about π-phase shifted) with respect to the backwards traveling wave [5]. For the configuration here (illustrated in Fig. 3(c)) the backwards and forward waves are also out-of-phase, however unlike for plasmonic structures, the sideways and backwards waves are in-phase in dielectric networks (see Fig. A2 in Appendix B). A simplified model for wave propagation in a resonant guided wave network (as developed in [5]) shows that these phase properties of the power splitting elements lead to the same interference condition that enhances the quality factor of the local resonance in the 2-by-2 RGWN.

We can also design equal power splitting structure with an all-dielectric scattering element when the scattering element is an air void surrounded by a Si cladding at the intersection of two 180 nm wide Si slab waveguides. Figure 4(a) shows that the power splitting between terminals equalizes for scattering elements with radius of 140 nm and cladding layer thickness of 60 nm. The splitting figure of merit ($FOM_{split}$) stays very high when the cladding thickness is varied up to 120nm. The fraction of scattered power is 0.6% for the best fit to equal power splitting, and stays very small (under 1.5%) for the rest of the parameter range of equal power splitting, as shown in Fig. 4(b). For this configuration of choice the bandwidth of operation is 290 THz, as observed from Fig. A3(a) in the Appendix B. Even though reflection and

#163588 - $15.00 USD Received 23 Feb 2012; revised 26 Mar 2012; accepted 26 Mar 2012; published 24 Apr 2012

transmission are out-of-phase (see Fig. A3 in Appendix B), similar to the phase distribution between terminals in plasmonic structures, the difference between the side and back terminals varies between 0.5π and 0.75π for cladding layer thickness values between 60 nm and 120 nm, respectively. While this is different from the π phase observed in plasmonic structures, it could be useful for designing other optical functions with RGWNs. Finally, broadband power splitting is evident in Fig. 4(c) (see also Media 2 for the power splitting dynamics), as a pulse of a few optical cycles equally splits in a junction of two 180 nm wide Si slab waveguides coupled to a 120 nm radius air void with a 60 nm Si cladding layer.

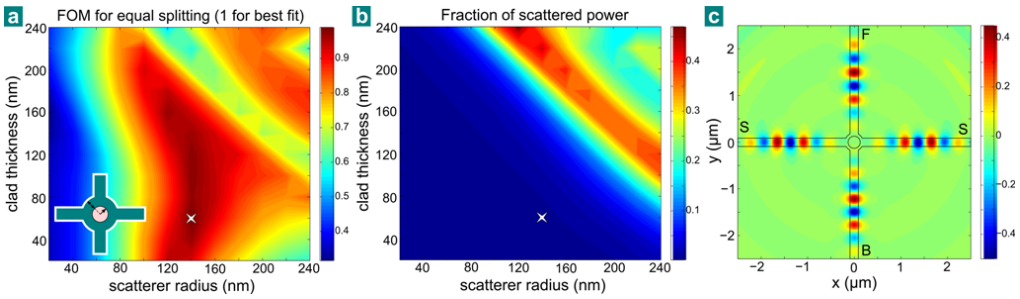


Fig. 4. Power splitting at the intersection of two 180 nm wide Si-air slabs modified by a radial etch scattering element at the junction: (a) FOM of equal splitting and (b) Fraction of scattered power as a function of the air particle radius and the Si cladding layer thickness. c) snapshot of the E-field out-of-plane component at the incidence of equal power splitting for a pulse excitation with the lowest TE polarization mode from terminal 'B' (Media 2). The intersection of the two 180 nm Si slabs is modified with a 140 nm radius air particle and 60 nm cladding layer as indicated by the structure overlay, and also by a white star on the parameter space in figures 'a' and 'b'. λ = 1.5μm.

Analysis of two-dimensional structures shows that by properly design of the scattering element, equal power splitting over wide band of frequencies is achievable. Despite the higher scattering loss, bending loss and lower bandwidth of operation than similar plasmonic structures, dielectric resonant guided wave networks exhibit much lower modal attenuation. After studying the idealized two-dimensional configurations, which indicate that resonant guided wave networks based on non-plasmonic waveguides are indeed possible, the next section examines three-dimensional dielectric scattering structures.

## 4. Analysis of three dimensional dielectric based scatterers

In this section we examine three-dimensional models for dielectric resonant guided wave networks fabricated in Si layers on thick layers of $SiO_2$. Rib waveguides were chosen here, rather than the ridge ones, because of their tighter modal confinement. Rib waveguides can be fabricated by selectively etching a thin Si layer on $SiO_2$ on a silicon-on-insulator (SOI) wafer after a lithography step. While examining the full range of the structural parameters might reveal the most optimized device, it is more instructive to fix some of the dimensions and study the system behavior while changing a smaller set of parameters, as we also did for the 2D case. We assign to the rib thickness (Si layer thickness) typical available dimensions and the rib width to the one that achieves the highest confinement of the lowest waveguide mode. We choose the Si layer thickness to be 220 nm, a typical dimension of commercially available SOI wafers. In the asymptotic case where the rib thickness is very large, which corresponds to the idealized 2D slab case, the lowest mode is the TE mode (the dominant E-field transversal component is out-of-plane), as discussed in the previous sections. As the rib thickness is reduced here to 220 nm the lowest mode becomes TM mode (the dominant E-field transversal component is in-the-plane). The cross-section of this lowermost mode is minimized for rib widths around 500 nm. For this rib cross-section (220 nm × 500 nm) the only two propagating modes are the lowest TE and the lowest TM, however the TM one would be the mode of choice here, having the higher effective index.

#163588 - $15.00 USD Received 23 Feb 2012; revised 26 Mar 2012; accepted 26 Mar 2012; published 24 Apr 2012

For the intersection of two (220 nm × 500 nm) rib waveguides, close to equal power splitting is achieved when modifying the junction with a cylindrical Au scattering particle, 125 nm in radius, and with a Si cladding layer thickness of up to 350 nm; the best figure of merit achieved is ($FOM_{split}$ = 0.91), inferred from the results in Fig. 5(a). For these parameters the fraction of scattered power is about 20% (see Fig. 5(b)). These achievable merits will enable the operation of an RGWN (as will be shown later on), even though they are not optimized, and in comparison to the idealized case they highlight the fact that the scattering element also couples light to radiation. This further illustrates that for dielectric waveguides with scatterers at the junctions, the dominant loss mechanism is not material-related propagation loss in the waveguides but radiation loss at the junctions. The phase distribution of the terminal outputs is consistent with that of the plasmonic X-junction, since the mode here is the lowest TM mode, as given in the Appendix B (see Fig. A4). The equal power split of a pulse of few optical cycles and also the formation of a local resonance, similar to the ones observed in the plasmonic case, is evident from Fig. 5(c) (also see Media 3 for the network dynamics).

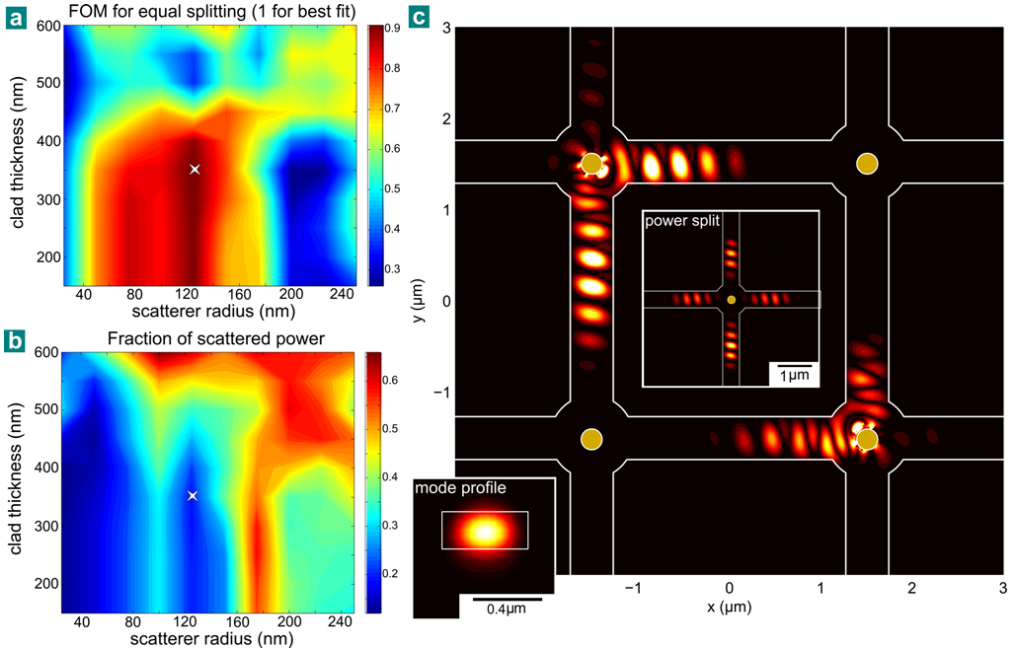


Fig. 5. Power splitting at the intersection of two 500 nm × 220 nm (width × thickness) Si rib waveguides modified by a cylindrical Au scattering element at the junction: (a) FOM of equal splitting and (b) fraction of scattered power as a function of the air particle radius and the Si cladding layer thickness. c) power snapshot for a 2x2 RGWN composed of four power splitting elements with 125 nm Au particle radius and 350 Si cladding layer (Media 3). The monitor plane is 100nm above the Si-SiO2 interface. A snapshot of the power splitting at one element and the modal cross-section are brought as insets. λ = 1.5µm.

A similar investigation of a high contrast dielectric scattering particle formed by creating an air void at the waveguide junction, which replaces the Au gives a very poor side power transmission maximum of a 6% (compared to 18% for three-dimensional Au scattering elements, and 25% in the ideal case), and very high scattering power of 35%. These merits where also obtained when varying the rib width in the range between 300 nm and 600 nm, where only the lowest TM mode exists and its confinement is maximal. It is possible that with more complex scattering topologies (e.g., multiple radial and concentric high contrast Bragg layers) or for a different Si layer thickness, equal power splitting could be obtained also for an all dielectric scattering element.

#163588 - $15.00 USD Received 23 Feb 2012; revised 26 Mar 2012; accepted 26 Mar 2012; published 24 Apr 2012

Comparison of the attenuation of dielectric-based and plasmonic resonant guided wave networks indicates that the high attenuation associated with plasmonic waveguides can be mitigated by using all dielectric structures. As a rough merit for comparison between the attenuation in plasmonic and dielectric based RGWNs we examine the major attenuation mechanisms: intrinsic modal attenuation for plasmonics versus scattering loss at the junctions for dielectric waveguides. For a network of two-dimensional slab waveguides with circular air scattering elements at the junctions (0.6% scattering loss per junction) with 10μm spacing between them the net decay length in the network is 600 μm - an order of magnitude larger than the typical net decay in a plasmonic network, which is limited by the 40 μm decay length in an MIM waveguide (of about 200 nm air gap). For the Au based scattering elements, both for the two-dimensional slab and three-dimensional rib waveguides, the decay length (120 μm and 20 μm, accordingly) is slightly better in comparison to their plasmonic waveguide counterparts (e.g., two-dimensional metal-insulator-metal waveguide with 40 μm and 3D-grooves with 10 μm modal decay length).

## 5. Conclusion

In this paper, resonant guided wave network design is shown to have a broader scope than plasmonics and is possible for photonic waveguide materials by modifying waveguide intersections with scattering elements. Possible realizations for the equal-power splitting element, a key enabler of this design, were proposed and studied based on a Au or dielectric (void) encapsulated particle in dielectric waveguide intersections. For realistic implementations, a rib waveguide network and Au-based scattering particle design is preferential to the all-dielectric system. These dielectric waveguides based RGWNs alleviate the high attenuation associated with plasmonics and allow for greater compatibility with photonic circuitry technology, marking a path for new network design possibilities.

## Appendix A: Elaborated description of the calculation depicted in Fig. 2(d)

In Fig. 2(d) the blue line describes the fraction of the power that was not coupled back to the terminals when excited from one of the terminals using TM1 mode, i.e., the scattered power for TM1 excitation. It is calculated as ‘1’ minus the total transmission through the terminals. For the TE1 excitation, the transmission to the four terminals is composed of the two fractions of the power being coupled to both TE modes. The solid red line (referred to as “both TE modes”) is calculated as ‘1’ minus the total transmission to both TE modes (TE1+TE2), i.e., the scattered power for the TE1 excitation. The dashed red line (referred to as “not coupled back to TE1”) is calculated as 1 minus the power fraction being transmitted only to TE1 mode, which indicates if the RGWN could be operated based only on TE1. The difference between the two red curves is the power coupled to TE2 mode for TE1 excitation. Both the red curves are calculated with the same TE1 excitation, the solid curve is calculated using a linear monitor across the waveguide that calculates the total power through the waveguide, and the dashed curve is calculated using a point monitor at the center of the waveguide, where the TE2 field is zero.

## Appendix B.

Characteristics of equal power splitting for the plasmonic case (MIM waveguides intersection):

#163588 - $15.00 USD Received 23 Feb 2012; revised 26 Mar 2012; accepted 26 Mar 2012; published 24 Apr 2012

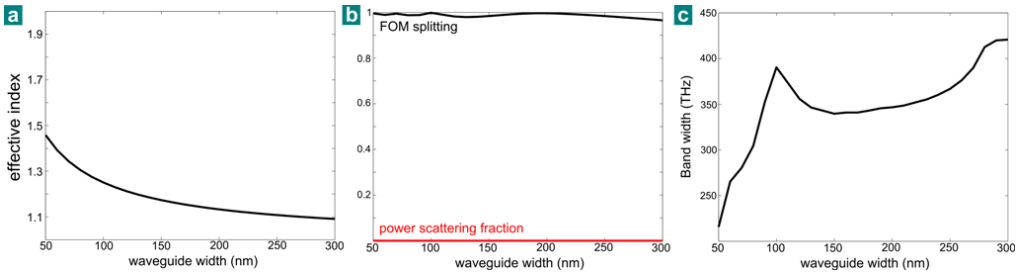


Fig. A1. Power splitting at the unmodified intersection of two equal width Au-air-Au (MIM) plasmonic waveguides at $\lambda = 1.5\mu m$ as a function of their gap width: a) effective index of the TM0 plasmonic mode of the MIM waveguide; b) FOM for equal power splitting and the fraction of scattered power; c) bandwidth of the transmission to sideways terminals.

Bandwidth and Phase characteristics of power splitting in the 2D case with metal scattering particle:

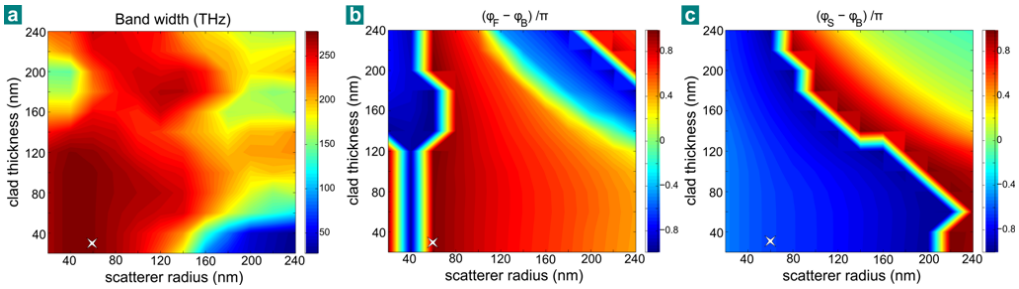


Fig. A2. Power splitting at the intersection of two 180nm wide Si-air slabs modified by a radial Au particle at the junction: a) bandwidth of the transmission to sideways terminals; phase difference of the split wave between the outputs of the (b) forward and backwards terminals and (c) sideways and backwards terminals.

Bandwidth and Phase characteristics of power splitting in the 2D case with air scattering particle:

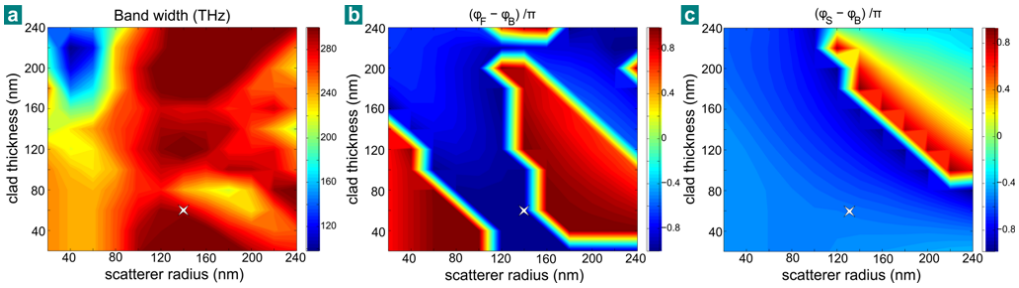


Fig. A3. Power splitting at the intersection of two 180 nm wide Si-air slabs modified by a radial etch scattering element at the junction: a) bandwidth of the transmission to sideways terminals; phase difference of the split wave between the outputs of the (b) forward and backwards terminals and (c) sideways and backwards terminals.

Phase characteristics of power splitting in the 3D case with metal scattering particle:

#163588 - $15.00 USD Received 23 Feb 2012; revised 26 Mar 2012; accepted 26 Mar 2012; published 24 Apr 2012

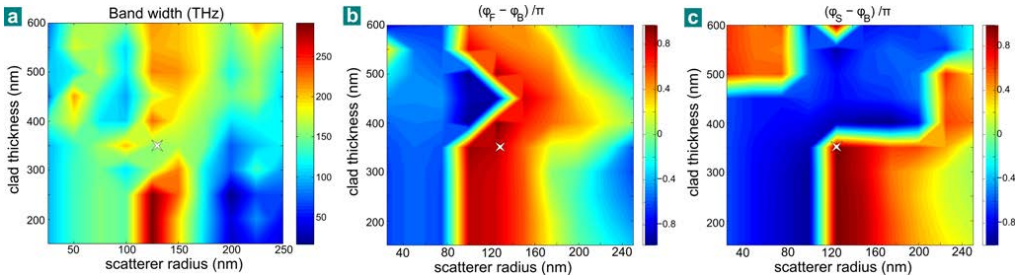


Fig. A4. Power splitting at the intersection of two (500 nm × 220 nm) Si rib waveguides modified by a cylindrical Au scattering element at the junction: a) bandwidth of the transmission to sideways terminals; phase difference of the split wave between the outputs of the (b) forward and backwards terminals and (c) sideways and backwards terminals.

For the 3D realization studied here the bandwidth maximization was not set as a design goal, since the problem was already more constraint than in the 2D cases. However, the bandwidth figure of merit over the parameter space is given in Fig. A4(a) for completeness. It suggests that for designs in which the bandwidth of operation should be maximized a thinner clad layer is preferable.

**Acknowledgments**

We wish to acknowledge the support from the Office of Basic Energy Sciences under Contract No. DE-FG02-07ER46405. E. F. wishes to acknowledge K. McCandless useful comments on text.

#163588 - $15.00 USD Received 23 Feb 2012; revised 26 Mar 2012; accepted 26 Mar 2012; published 24 Apr 2012